Inclusive reaction ^{93}Nb($\vec{p}$,α) at an incident energy of 160 MeV

S. S. Dimitrova,[1,*] A. A. Cowley,[2,3,†] J. J. van Zyl,[2] E. V. Zemlyanaya,[4] and K. V. Lukyanov[4]
[1]*Institute for Nuclear Research and Nuclear Energy, Bulgarian Academy of Sciences, 1784 Sofia, Bulgaria*
[2]*Department of Physics, Stellenbosch University, Private Bag X1, Matieland, 7602, South Africa*
[3]*iThemba Laboratory for Accelerator Based Sciences, P. O. Box 722, Somerset West 7129, South Africa*
[4]*Joint Institute for Nuclear Research, 141980 Dubna, Russia*
(Received 19 December 2013; revised manuscript received 4 February 2014; published 20 March 2014)

The inclusive ^{93}Nb($\vec{p}$,α) reaction to the continuum was investigated at an incident energy of 160 MeV. Emission-energy angular distributions for cross sections as well as analyzing powers were explored. A range of scattering angles from 15° to 60° (lab.) was covered and α-particle emission energies from ≈30 MeV to the kinematic limit were measured. As in our earlier work, the experimental distributions were compared with a multistep direct theory combined with a knockout reaction mechanism as the terminating step in the α-particle emission. Reasonable agreement between the theoretical predictions and the experimental double-differential cross section and analyzing-power angular distributions were obtained.

DOI: 10.1103/PhysRevC.89.034616 PACS number(s): 25.40.Hs, 24.50.+g, 24.60.Gv, 24.70.+s

I. INTRODUCTION

Pre-equilibrium nuclear reactions have been studied extensively over many years, as represented by a few examples [1–3], and impressive progress in our understanding of the basic mechanism has been made. Nevertheless, some important details of the reaction mechanism are still obscure and, consequently, need to be better explored. Recently it was pointed out that at incident energies in the 100- to 200-MeV range, proton-induced α-particle pre-equilibrium emission seems to display an enhanced cross-section yield towards lower emission energies compared to standard theoretical predictions [4,5]. It was speculated that this is due to inelastic excitations to states which subsequently undergo α-particle decay. It would be useful to investigate this idea further, and this is implicitly explored in the present work, which could show the need for inclusion of an additional reaction mechanism as postulated in Refs. [4,5].

For (p,^{3}He) pre-equilibrium reactions in the same incident energy range, the reaction mechanism is described fairly accurately in terms of a series of multiple intranuclear nucleon-nucleon collisions, which finally end in a dinucleon pickup step to produce the emitted ^{3}He [6–9]. The analyzing power proves to be especially sensitive to the progression of intranuclear collisions, and the number of steps preceding the pickup affects the appearance of the analyzing angular distributions very prominently. The systematic trends of the cross section, as well as analyzing-power angular distributions with incident and emission energy, are predicted reasonably accurately. Although the trends with incident and emission energy of the analyzing-power distributions differ markedly for two target nuclei (^{59}Co and ^{93}Nb) which were investigated, the predictions of the theoretical formulation clearly point to involvement of the same basic reaction mechanism in both cases [8]. It is reasonable to assume that the two targets are representative of atomic nuclei in general in their response to the (p,^{3}He) reaction and that reaction mechanism dependence on target mass is trivial.

A similar multiple intranuclear scattering reaction model has also previously been successfully tested for the ^{59}Co(p,α) reaction in the same range of incident energies [10]. However, instead of a final two-nucleon pickup as in (p,^{3}He), based on dynamical and kinematic arguments, it was postulated that cluster knockout would be a more likely final step in the (p,α) process. Only experimental cross-section data, which were to a certain extent predicted reasonably well by the theoretical formulation, were available for the earlier studies. Because of the greater sensitivity of analyzing power to the reaction mechanism, it is desirable to extend the work to the investigation of the (p,α) reaction with polarized protons as presented in this paper. The reaction ^{93}Nb(p,α) at an incident energy of 160 MeV was selected as a representative choice for this purpose.

In Sec. II the experimental setup and design considerations are presented. Section III comprises a brief overview of the salient features of the theoretical treatment, with a description of the folding technique to generate optical potentials used to calculate appropriate distorted waves for the incident proton and the outgoing α particles. The results are presented and discussed in Sec. IV. Finally, a summary and conclusions are given in Sec. V.

II. EXPERIMENTAL PROCEDURE

The cyclotron facility iThemba Laboratory for Accelerator Based Sciences (LABS), Faure, South Africa, was used in the study. An external source fed a polarized ion beam into an injector cyclotron which accelerated protons to a maximum energy of 8 MeV. Further acceleration in the main separated sector cyclotron delivered a polarized proton beam of 160 ± 0.5 MeV. The accelerator system and the experimental equipment used in this study have been described elsewhere [11].

The current ($\vec{p}$,α) data were collected simultaneously with the ($\vec{p}$, ^{3}He) study reported previously [9], and we followed

*sevdim@inrne.bas.bg
†aac@sun.ac.za

the techniques described in our earlier work very closely [7,8]. Consequently, only a brief description is given here for ease of reference. Note that we use the symbol p interchangeably also for polarized protons, as would be clear from the context.

Two detector telescopes, mounted inside a 1.5-m-diameter scattering chamber, were used. Each telescope consisted of a 500-μm silicon surface barrier detector followed by a NaI(Tℓ) crystal which was connected to a photomultiplier tube. Standard ΔE–E particle identification techniques were employed to select particles scattered from a target mounted at the center of the scattering chamber. Tantalum collimators, thick enough to stop scattered particles of interest (approximately 3 mm thick with a 14-mm-diameter hole) defined an active solid angle of 1.13 msr for each telescope. Lighter reaction products (protons, deuterons, and tritons) would normally penetrate the tantalum and therefore enter the telescopes. The flux of these particles was attenuated by brass collimators with a slightly larger hole in front of the tantalum.

Systematic errors on the measurement of the analyzing power were minimized by following standard methods, such as placing the two detector telescopes at symmetric scattering angles on opposite sides of the beam during data taking and switching the direction of the polarization of the incident protons from up to down at 10-s intervals.

The polarization of the beam was determined regularly by scattering of the beam from a ^{12}C foil in the scattering chamber at 19° where the analyzing power for $p+^{12}$C elastic scattering at 160 MeV is large (0.92) and accurately known [12]. The difference in the polarization between the two orientations was usually less than 10%, but different values as determined experimentally were used for the two polarization orientations to calculate analyzing-power values. The polarization ranged from 65 to 85% during the experiment and changed slowly as ion source operating conditions drifted.

Energy response of the silicon surface barrier detectors was calibrated with a ^{228}Th α-particle source, and those of the NaI(Tℓ) detector elements were based on the kinematics of the elastic-scattering reactions ^{1}H$(p,p)^{1}$H and ^{12}C$(p,p)^{12}$C from a thin polyethylene target. These calibrations for protons in the telescope also provide energy values for α particles if the difference in the response of these ejectiles with the NaI(Tℓ) assembly is taken into account [13]. A light-emitting diode pulser system monitored gain drifts in the photomultiplier tubes of the NaI detectors, allowing corrections to be made during analysis. Overall uncertainty was approximately 4% in the α-particle energy scale.

Two self-supporting foils of natural isotopic composition (100% occurrence of the isotope of interest) ^{93}Nb targets which were used. These had thicknesses of 2.6 and 8.6 mg/cm^2. The uncertainty in the thicknesses of the targets (up to 7%) is the main contribution to the systematic error on the cross-section data.

Standard electronics were used and data were collected and monitored on an online system and stored for subsequent offline replay of the data. Data were obtained for α-particles emission energies from a threshold of ≈30 MeV up to the kinematic limit and scattering angles from 15° to 60° (lab.) were covered.

III. THEORETICAL ANALYSIS

Analogously to the calculation of the $(p,^3\mathrm{He})$ inclusive reaction in our previous work [6–9], we also treat the (p,α) reaction as occurring in a series of intranuclear N-N steps preceding a final process in which the α particle is emitted.

For a (p,α) reaction in the present work, in addition to the possibility of three-nucleon pickup, knockout has to be considered as an important component of the reaction mechanism. As the simplest process leading to α-particle emission, the incident proton can knock out an α cluster (or, alternatively, pick up three nucleons) directly from the target in a single step. We refer to such an event as a first-step (p,α) reaction.

In higher-order steps, final emission of an α particle takes place after a variable number of intranuclear nucleon collisions. In our notation a two-step reaction is symbolically indicated as (p,p',α) and a three-step reaction as (p,p',p'',α).

The theory applied to the (p,α) reaction is based on the multistep direct theory of Feshbach, Kerman, and Koonin (FKK) [14] for the intranuclear collisions, which lead up to a final α-particle emission. The last step is treated in a distorted-wave Born approximation (DWBA).

The theoretical formulation has been described extensively in our earlier publications and references therein. However, to highlight some subtle, but inconsequential, modifications required for application to this study, we describe the main expressions describing the theory in the subsection which follows. For clarity we use a notation which is analogous to that of Refs. [8,9]. Of course, the notation is adjusted to be appropriate for the present application to a (p,α) reaction.

A. Differential cross sections

The double-differential cross section is written in the standard way to emphasize its relationship to solid angle $d\Omega$ and emission energy dE acceptance. This is expressed as

$$\frac{d^2\sigma}{d\Omega dE} = \left(\frac{d^2\sigma}{d\Omega dE}\right)^{1-\mathrm{step}} + \left(\frac{d^2\sigma}{d\Omega dE}\right)^{2-\mathrm{step}} + \cdots, \quad (1)$$

where, as mentioned earlier, the first step cross section is taken as a direct reaction calculated in terms of the DWBA. This term is given by

$$\left(\frac{d^2\sigma}{d\Omega dE}\right)^{1-\mathrm{step}} = \sum_{N,L,J} \frac{(2J+1)}{\Delta E} \frac{d\sigma^{\mathrm{DW}}}{d\Omega}(\theta,N,L,J,E), \quad (2)$$

at scattering angle θ, where the summation runs over the target states with single-particle energies within a small interval $(E-\Delta E/2, E+\Delta E/2)$ around the excitation energy E. If the DWBA calculation is treated as a knockout, quantum numbers N, L, and J refer to the α cluster bound in the target, otherwise to those of the three-nucleon system which is picked up. The differential cross sections $\frac{d\sigma^{\mathrm{DW}}}{d\Omega}$ to particular (N,L,J) states are calculated using the code DWUCK4 [15].

The multistep cross sections, which are appropriate for the second and higher steps of the (p,α) reaction, are expressed as

$$\left(\frac{d^2\sigma}{d\Omega dE}\right)^{\text{multistep}} = \sum_{n=2}^{n_{\max}}\sum_{m=n-1}^{n+1}\int\frac{d\mathbf{k}_1}{(2\pi)^3}\int\frac{d\mathbf{k}_2}{(2\pi)^3}\cdots\int\frac{d\mathbf{k}_n}{(2\pi)^3} \times\left(\frac{d^2\sigma(\mathbf{k}_f,\mathbf{k}_n)}{d\Omega_f dE_f}\right)\times\left(\frac{d^2\sigma(\mathbf{k}_n,\mathbf{k}_{n-1})}{d\Omega_n dE_n}\right)\times\cdots \times\left(\frac{d^2\sigma(\mathbf{k}_2,\mathbf{k}_1)}{d\Omega_2 dE_2}\right)\times\left(\frac{d^2\sigma(\mathbf{k}_1,\mathbf{k}_i)}{d\Omega_1 dE_1}\right)^{1-\text{step}}_{p,p'}, \quad (3)$$

where $\mathbf{k}_i$, $\mathbf{k}_n$, and $\mathbf{k}_f$ are the momenta of the initial, n^{th} and final steps. The number of reaction steps is indicated with the symbol n, the maximum number of reaction steps is $n_{\max}$, and m is the exit mode. Therefore the cross section associated with m is given leading to the emission of an α particle, and all steps prior to the final step are nucleon-nucleon collisions.

Clearly, the formalism separates calculation of multistep processes, such as one-step (p,α), two-step (p,p',α), and three-step (p,p',p'',α) reactions. As in previous work [7,8], intermediate steps which involve neutrons, such as (p,n,α), are ignored because we assume that different nucleons may be treated on an equal footing in the multistep part of the reaction. The effect of this approximation can be compensated for by a single renormalization of the relevant (p,p') and (p,p',p'') cross sections used in the calculations. The magnitude of the theoretical cross section is refitted to the experimental data anyway, as will be explained later, thus simplifying the earlier renormalization.

The theoretical (p,p') and (p,p',p'') double-differential cross section distributions which are required to calculate the contributions of the second- and third-step processes were derived from Refs. [10,16]. These cross-section distributions were extracted by means of a FKK multistep direct reaction theory, which reproduce experimental inclusive (p,p') quantities [16] on target nuclei which are close to those needed for this work, and in an appropriate incident energy range. Interpolations and extrapolations in incident energy and target mass were introduced to match the specific requirements accurately.

B. Analyzing-power distributions

The analyzing power in terms of protons polarized to a value P_+ in the positive (up) direction as defined by the Basel [17] and Madison [18] conventions, is given by

$$A_y = \frac{1}{P_+}\left(\frac{\sigma_L-\sigma_R}{\sigma_L+\sigma_R}\right), \quad (4)$$

where σ_L and σ_R are the double-differential cross sections for the emission of α particles to the left L and right R of the incident particle beam, respectively. An analogous expression holds when the proton polarization is flipped relative to the scattering plane. A fully polarized beam has a magnitude of unity.

The extension of the FKK theory from cross sections to analyzing power is described by Bonetti *et al.* [19]. The multistep expression for the analyzing power becomes

$$A_{\text{multistep}} = \frac{A_1\left(\frac{d^2\sigma}{d\Omega dE}\right)^{1-\text{step}} + A_2\left(\frac{d^2\sigma}{d\Omega dE}\right)^{2-\text{step}}+\cdots}{\left(\frac{d^2\sigma}{d\Omega dE}\right)^{1-\text{step}}+\left(\frac{d^2\sigma}{d\Omega dE}\right)^{2-\text{step}}+\cdots}, \quad (5)$$

with A_i, $\{i=1,2,\ldots\}$ referring to analyzing powers for the successive multisteps.

C. Optical potentials in the DWBA calculation

Important ingredients in the theoretical description of the nuclear reaction properties are the optical potentials, which take into account the interaction between projectile and target, and between the ejectile and the heavy residual nucleus, respectively. In general, the potentials contain volume V and spin-orbit V_{SO} parts, which are both complex and expressed as

$$U(\mathbf{r}) = V(\mathbf{r}) + V_{\text{SO}}(\mathbf{r})\,\mathbf{L}\cdot\mathbf{S}, \quad (6)$$

where r is the relative radial coordinate, $\mathbf{L}$ the angular momentum, and $\mathbf{S}$ the intrinsic spin of the projectile. Note that, in the ^{4}He case, $\mathbf{S}=0$, and therefore the spin-orbit term falls away.

We treat the volume part of the optical potentials in the initial and the exit channels on the same footing by application of the hybrid nucleus-nucleus optical potential.

The hybrid nucleus-nucleus optical potential [20] has real and imaginary parts,

$$U(\mathbf{r}) = N^R V^{\text{DF}}(\mathbf{r}) + iN^I W(\mathbf{r}), \quad (7)$$

which generally depend on the radius-vector $\mathbf{r}$ connecting centers of the interacting nuclei. The parameters N^R and N^I correct the strength of the microscopically calculated real V^{DF} and imaginary W constituents of the whole potential. The real part V^{DF} is a double-folding potential that consists of direct and exchange components,

$$V^{\text{DF}}(\mathbf{r}) = V^D(\mathbf{r}) + V^{\text{EX}}(\mathbf{r}), \quad (8)$$

with

$$V^D(\mathbf{r}) = \int d\mathbf{r}_p\, d\mathbf{r}_t\, \rho_p(\mathbf{r}_p)\rho_t(\mathbf{r}_t)v^D_{NN}(\mathbf{s}). \quad (9)$$

The exchange potential is

$$V^{\text{EX}}(\mathbf{r}) = \int d\mathbf{r}_p\, d\mathbf{r}_t\, \rho_p(\mathbf{r}_p,\mathbf{r}_p+\mathbf{s})\rho_t(\mathbf{r}_t,\mathbf{r}_t-\mathbf{s}) \times v^{\text{EX}}_{NN}(s)\exp\left[\frac{i\mathbf{K}(\mathbf{r})\cdot\mathbf{s}}{M}\right], \quad (10)$$

where $\mathbf{s}=\mathbf{r}+\mathbf{r}_t-\mathbf{r}_p$ is the vector between the projectile and target nucleons. The reduced mass coefficient is $M = A_pA_t/(A_p+A_t)$, where A_p and A_t refer to the projectile and target atomic mass numbers. The radial part of the nucleus-nucleus momentum $K(r)$ is determined as follows:

$$K(r) = \left\{\frac{2Mm}{\hbar^2}[E - V^{\text{DF}}(r) - V_c(r)]\right\}^{1/2}. \quad (11)$$

where V_c is the Coulomb potential and m is the nucleon mass. The quantities $\rho_p(\mathbf{r}_p)$ and $\rho_t(\mathbf{r}_t)$ are their density distributions, $\rho_p(\mathbf{r}_p,\mathbf{r}_p+\mathbf{s})$ and $\rho_t(\mathbf{r}_t,\mathbf{r}_t-\mathbf{s})$ are the density matrices, which are approximated as in Ref. [21]. The effective NN potentials v^D_{NN} (of CDM3Y6-type) are based on the Paris NN potential,

$$v^D_{NN}(E,\rho,s) = g(E)F(\rho)\sum_{i=1}^{3} N_i \frac{\exp(-\mu_i s)}{\mu_i s}. \qquad (12)$$

The energy and density dependencies are, respectively,

$$\begin{aligned} g(E) &= 1 - 0.003E/A_p, \\ F(\rho) &= C[1+\alpha e^{-\beta\rho} - \gamma\rho], \\ \rho &= \rho_p(\mathbf{r}_p) + \rho_t(\mathbf{r}_t). \end{aligned} \qquad (13)$$

The parameters in Eq. (12) and Eq. (13) are defined in Ref. [22].

For the potential in the $p+^{93}$Nb channel, in Eqs. (9), (10), and (13) one should exclude the respective functions $\rho_p(\mathbf{r}_p)$ together with the elementary volumes $d(\mathbf{r}_p)$. Also, in Eqs. (14) and (15) below, $\rho_p(\mathbf{q})$ will not appear.

For the initial channel calculations, ρ_t for ^{93}Nb was taken as the standard Fermi form, with parameters from Ref. [23]. In the exit channel a Fermi-form density with parameters from Ref. [24] was adopted for ^{90}Zr, and the ^{4}He density from Ref. [25] was used.

The imaginary part of the optical potential $W(\mathbf{r})$ in Eq. (7) may have the same form as its real counterpart $V^{\rm DF}$ or can be calculated separately within the high-energy approximation [26] as it was developed in Ref. [20].

The microscopic optical potential obtained in the high-energy approximation in the momentum space has the following form:

$$U^H_{\rm opt}(\mathbf{r}) = -\frac{E}{k}\bar{\sigma}_N(i+\bar{\alpha}_N)\frac{1}{(2\pi)^3} \times \int d\mathbf{q} e^{-i\mathbf{q}\cdot\mathbf{r}}\rho_p(\mathbf{q})\rho_t(\mathbf{q})f_N(q). \qquad (14)$$

Here the NN total scattering cross section $\bar{\sigma}_N$ and the ratio of real to imaginary parts of the forward NN amplitude $\bar{\alpha}_N$ are averaged over the isospins of the projectile and target nuclei. They are parameterized as given in Refs. [27,28]. The NN form factor is taken as $f_N(q) = \exp(-q^2\beta_N/2)$ with the slope parameter $\beta_N = 0.219\,\mathrm{fm}^2$ [29]. In fact, we used only the imaginary part of Eq. (14) transformed to the form

$$W^H(r) = -\frac{1}{2\pi^2}\frac{E}{k}\bar{\sigma}_N\int_0^\infty j_0(qr)\rho_p(q)\rho_t(q)f_N(q)q^2dq. \qquad (15)$$

Details about the calculations of the hybrid optical potential are presented in Refs. [20,22,30,31].

The hybrid optical potential as described above has already been successfully applied, e.g., in Refs. [32–35] for the analysis of elastic-scattering data of light exotic nuclei.

The shape of the analyzing power is rather sensitive to the spin-orbit part of the optical potential in the initial channel. Good agreement with the experimental data was obtained by using for protons a Woods-Saxon shape of the real part of $V_{\rm SO}(r)$. We used the parameters listed in Ref. [36]. The renormalization constants N^R and N^I in Eq. (7) in the initial channel are kept equal to unity, while their values for the exit channel were adjusted to follow the emission-energy trend of the experimental analyzing-power data [see Table (I)].

TABLE I. Values of the renormalization constants N^R and N^I in Eq. (7) for the outgoing channel.

$E_{\rm out}$ (MeV)	158	142	130	82
N^R	1.0	0.8	0.8	0.8
N^I	0.5	0.1	0.1	0.1

Our treatment of N^R and N^I in the exit channel as free parameters which are fitted to the data is consistent with the procedure followed in Ref. [34]. Note that we find a need to use a value of N^I of 0.5 at $E_{\rm out} = 158$ MeV, as opposed to values of 0.1 for all other sets. This is counterintuitive and not understood at all. Clearly, the values found in our present investigation, and the trend observed as a function of emission energy, need further theoretical analysis and complementary experimental studies for proper evaluation and interpretation.

D. Reaction mechanism

The mechanism of the direct (p,α) reaction has been debated intensively over the years. For example, in Ref. [37] the authors show that calculations assuming pickup of a triton and knockout of an α particle equally well fit the angular distribution and the analyzing power of the ^{90,92}Zr(p,α) reaction to the ground state and the first few excited states, while in Ref. [38] the knockout mechanism is preferred for describing transitions to the continuum.

To address this problem for the reaction which we study we perform DWBA calculations assuming both reaction mechanisms and compare the theoretical results with the experimental data for the differential cross section and the analyzing power for 158-MeV outgoing energy, where the first step process dominates and for 130 MeV, where the second step plays an important role. Numerically the difference between both types of calculations lies in the form factor, and the incoming and the outgoing distorted waves are calculated using the same optical model potentials for protons and α particles, respectively. The proton-triton binding potential has a Woods-Saxon shape with geometrical parameter $r_0 = 1.488$ fm and $a = 0.144$ fm as recommended in Ref. [39], whereas to generate the α-particle form factor we use the generally accepted geometrical parameter values of $r_0 = 1.25$ fm and $a = 0.65$ fm. The theoretical double-differential cross sections are scaled to fit the experimental data for $E_{\rm out} = 158$ MeV at low outgoing angles θ in both cases. The scaling factors are kept unchanged throughout the rest of the calculations at other emission energies.

In Fig. 1 we compare the results for both reaction mechanisms at high outgoing energy. The slope of the differential cross section calculated assuming α-particle knockout is closer to the experimental data, while for the analyzing power the

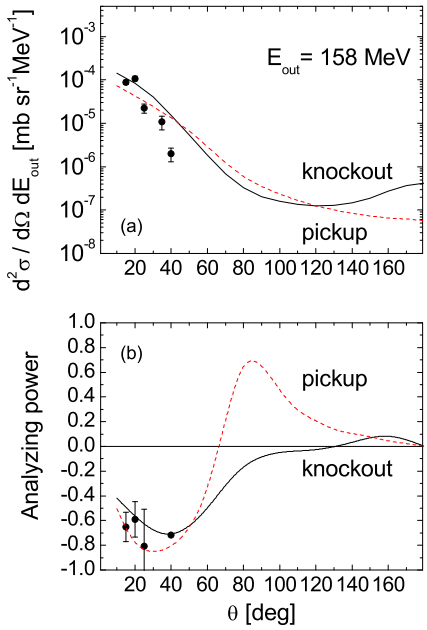

FIG. 1. (Color online) Double-differential cross sections (a) and analyzing power (b) as a function of scattering angle θ for the ^{93}Nb(p,α) reaction at an incident energy of 160 MeV and an α-outgoing energy of 158 MeV. Theoretical calculations assuming a knockout mechanism are denoted by solid lines and those using a pickup mechanism by dashed lines.

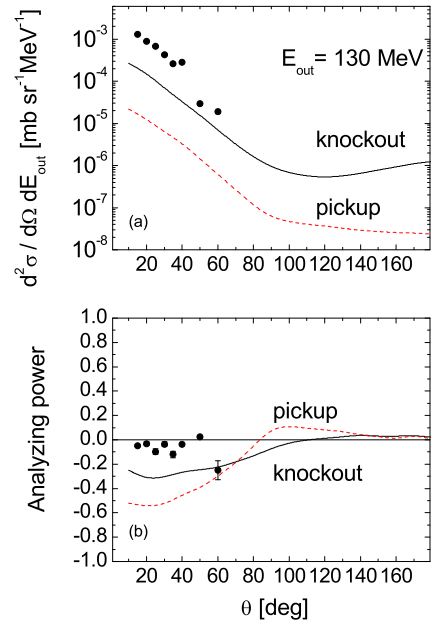

FIG. 2. (Color online) The same as in Fig. 1 for $E_{\rm out} = 130$ MeV.

available experimental data do not provide enough information for an exclusive choice.

For reactions with lower outgoing energies for which the $(p,p'\alpha)$ process starts to dominate, like in the $E_{\rm out} = 130$ MeV case, the difference between the predicted results for the two mechanisms becomes more prominent, as shown in Fig. 2. Although the indicated theoretical cross-section values are considerably too low for both postulated mechanisms, it should be kept in mind that the overall absolute scale is fairly arbitrary, as will be discussed later. However, the relative difference in cross section for the two processes is as shown. Of course, the normalization does not directly affect the analyzing power, which consists of a ratio of cross sections. Clearly the comparison between the theory and the experimental distributions appears to be somewhat better for the knockout mechanism. Thus we will adopt the knockout mechanism as appropriate to the rest of our study of the ^{93}Nb(p,α) pre-equilibrium reactions.

IV. RESULTS AND DISCUSSION

Double-differential cross section and analyzing-power angular distributions for the ^{93}Nb(p,α) reaction at an incident energy of 160 MeV are displayed in Fig. 3 for various outgoing energies of the α particles.

Experimental data are available for outgoing energies starting from 158 MeV (with 166 MeV as a kinematic limit due to a positive Q value) down to about 30 MeV. We have chosen the ones shown in the figure because they are representative for the contribution of the different steps to the total differential cross section and analyzing power respectively. The theory reproduces the general trend of the experimental quantities reasonably well, especially if we keep in mind that the accuracy of the calculations is limited to some extent by uncertainties inherent to the input ingredients of the theory, as implied in Sec. III.

All the theoretical cross-section distributions were normalized with a single factor extracted from the most forward angles of the angular distribution at an emission energy $E_{\rm out}$ of 158 MeV, for which the one-step reaction dominates, as explained in Sec. III D. Although this procedure is based on theoretical considerations, it is still somewhat arbitrary. Experimental uncertainties in, for example, the emission energy calibration would result in a systematic error in the measured cross section which rapidly gets worse towards the top end of emission energies. The reason is that the energy distribution of the cross section as function of emission energy drops very rapidly to zero as the kinematic limit is approached, whereas it varies considerably more slowly at lower emission energies. Our cross-section data at the highest emission energy is already in an energy range where a rapid variation occurs. This, combined with the experimental uncertainty in emission energy, could affect the reliability of the normalization procedure. Consequently, the fact that the cross sections appear to be mostly underestimated by the theory, especially at a lower outgoing energy, could to a large extent be an artifact of our normalization procedure. Of course, for relatively low emission energies there are other processes kinematically allowed which differ from only the ones we consider. Consequently, difficulties to reproduce the magnitude of the differential cross section is not very surprising. Of course, as was mentioned earlier, fortunately the analyzing power is unaffected by most of these complications.

Nevertheless, the fact that our present calculations for ^{93}Nb(p,α) at an incident energy of 160 MeV suggest a more

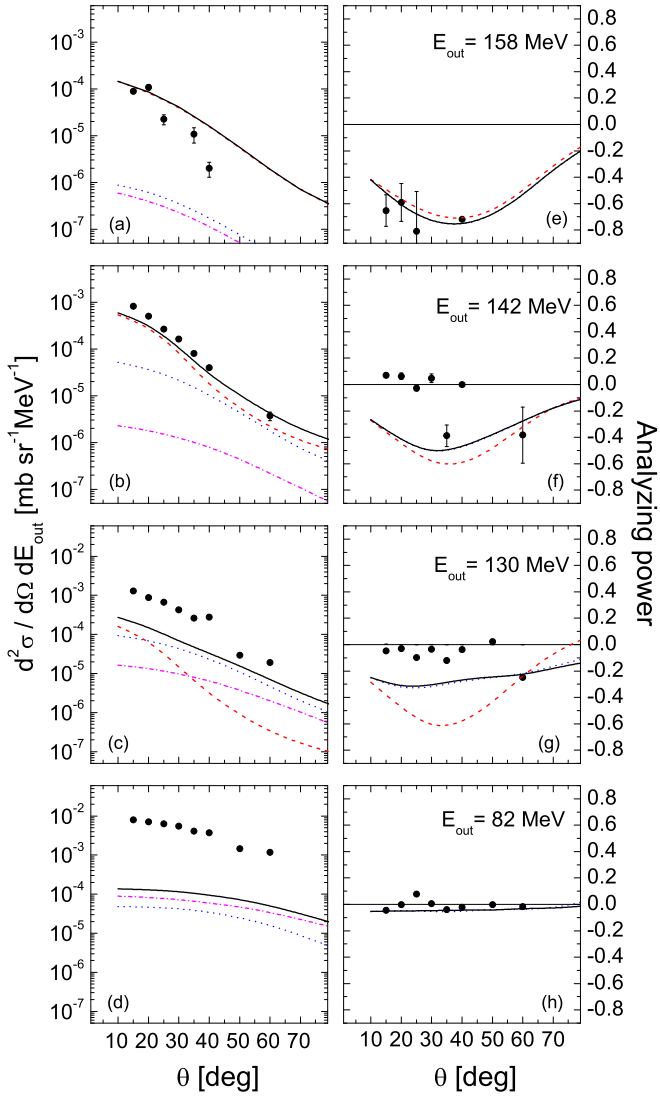

FIG. 3. (Color online) Double-differential cross sections [(a)–(d)] and analyzing power [(e)–(h)] as a function of scattering angle θ for the ^{93}Nb(p,α) reaction at an incident energy of 160 MeV and various α-particle outgoing energies $E_{\rm out}$ as indicated. Theoretical cross-section calculations for one step (— — —), two steps (· · · · ·), and three steps (— · — · —) are shown, with the sums of the contributions plotted as continuous curves. The experimental analyzing-power distributions are compared with theoretical calculations for a one-step reaction (— — —), a one-step plus a two-step reaction (· · · · ·), and a one- plus two- plus three-step reaction (solid lines). The experimental data are averaged over emission energy bins of 4 MeV and statistical error bars are shown where those exceed the symbol size.

rapid decrease of the cross section towards lower emission energy than observed experimentally, is consistent with an earlier study on ^{59}Co(p,α) at the same incident energy [10]. The results of the latter work were discussed in Ref. [5] and it was speculated that the observed phenomenon could be an indication of an additional reaction mechanism, namely inelastic excitation followed by sequential α-particle decay. However, whether such a process as postulated could be significant at emission energies as high as those of Fig. 3 still needs to be explored.

As may be seen in Fig. 3, the theory predicts that the relative contribution of the first-step reaction decreases as the emission energy drops, with higher steps becoming progressively more important towards lower emission energy. This is a general feature of multistep calculations, as was also found in our previous work [6–9]. Although the actual step which is dominant at a specific emission energy only influences the shape of the cross section relatively slightly, an appreciable contribution of higher steps affects the analyzing-power distribution profoundly. The trend is that the analyzing power tends towards zero at lower emission energy where higher steps become more important.

At the incident energy of 160 MeV of the present work, the analyzing power of the ^{93}Nb(p,α) reaction approaches zero very rapidly as the emission energy drops. It should be noted that results are only shown down to an emission energy of 82 MeV in Fig. 3, but below this outgoing energy the analyzing power remains essentially zero, thus conveying the same information regarding the dominant step in the reaction mechanism.

It is noteworthy that the experimental analyzing-power angular distributions do not follow the predicted trend as well as would be desirable, nor are the shapes of the experimental cross-section angular distributions accurately reproduced by the theory. However, one should keep in mind, as mentioned before, that the implementation of the theory suffers from uncertainties in the input ingredients of the formulation. Nevertheless, the overall prediction for analyzing power is reasonable.

For reasons which were mentioned in Sec. III D, we exclude the possible contribution of a pickup process. As may be concluded from the results shown in Figs. 1 and 2, inclusion of such a process is unlikely to resolve the observed problem with the relative cross-section magnitudes as a function of emission energy.

V. SUMMARY AND CONCLUSIONS

The reaction ^{93}Nb(p,α) at an incident energy of 160 MeV leading to ejectiles into the continuum of excitation was investigated. Double-differential cross section and analyzing-power angular distributions were measured between 15° and 60° at various emission energies.

The target nucleus was selected because it is a naturally occurring monoisotopic nuclide which is readily available and because earlier work suggests that the postulated reaction mechanism should not suffer from a drastic target-mass dependence.

The experimental results were compared with calculations of statistical multistep formulation in which each individual intra nucleon-nucleon collision in the sequence of steps may be terminated with emission of an α particle. The ejectile is assumed to originate from an α-cluster knockout in the final stage. The theoretical predictions roughly reproduce the angular distributions of the measured cross section and analyzing power as a function of α-particle emission energy. However, the trend of the absolute cross section appears to be a problem. Fortunately, this problem does not affect the analyzing power, which is essentially a ratio of cross sections.

Although not producing results which provide evidence of the reaction mechanism as clearly as our previous work on (p,^{3}He) reactions, the observed signatures of cross section and analyzing power are nevertheless reasonably consistent with those earlier conclusions. This suggests related reaction mechanisms for (p,^{3}He) and (p,α) reactions at comparable incident energies. It is tempting to speculate that the cross-section behavior points to the importance of an additional reaction mechanism, but this interpretation is not supported by the emission-energy trend of analyzing-power angular distributions.

Further studies of proton-induced α-particle emission into the continuum of outgoing energies are desirable. Additional theoretical refinement and development would also be very useful. In addition, experimental work at lower incident energy, where cross sections and analyzing powers are larger, together with polarized beams of much higher intensity, should provide data with improved accuracy. Such lower-uncertainty data would provide better guidance in the comparison with theoretical predictions.

ACKNOWLEDGMENTS

We thank V. K. Lukyanov for his valuable guidance during the development of the formulation of the folding potentials. The research of A.A.C. was funded by the National Research Foundation (NRF) of South Africa. The studies of S.S.D. were partially supported by the SARFEN grant of the Bulgarian Science Foundation. E.V.Z. and K.V.L were supported by the Russian Foundation for Basic Research (RFBR) under Grants No. 12-01-00396a and No. 13-01-00060a. This financial support is gratefully acknowledged.

[1] E. Gadioli and P. E. Hodgson, *Pre-Equilibrium Nuclear Reactions* (Oxford University Press, New York, 1991).
[2] A. J. Koning and J. M. Akkermans, Phys. Rev. C **47**, 724 (1993).
[3] A. J. Koning and M. C. Duijvestijn, Nucl. Phys. A **744**, 15 (2004).
[4] A. A. Cowley, EPJ Web of Conferences **21**, 09002 (2012).
[5] A. A. Cowley, EPJ Web of Conferences **38**, 13001 (2012).
[6] A. A. Cowley, G. J. Arendse, G. F. Steyn, J. A. Stander, W. A. Richter, S. S. Dimitrova, P. Demetriou, and P. E. Hodgson, Phys. Rev. C **55**, 1843 (1997).
[7] A. A. Cowley, G. F. Steyn, S. S. Dimitrova, P. E. Hodgson, G. J. Arendse, S. V. Förtsch, G. C. Hillhouse, J. J. Lawrie, R. Neveling, W. A. Richter, J. A. Stander, and S. M. Wyngaardt, Phys. Rev. C **62**, 064605 (2000).
[8] A. A. Cowley, J. Bezuidenhout, S. S. Dimitrova, P. E. Hodgson, S. V. Förtsch, G. C. Hillhouse, N. M. Jacobs, R. Neveling, F. D. Smit, J. A. Stander, G. F. Steyn, and J. J. van Zyl, Phys. Rev. C **75**, 054617 (2007).
[9] A. A. Cowley, J. J. van Zyl, S. S. Dimitrova, E. V. Zemlyanaya, and K. V. Lukyanov, Phys. Rev. C **85**, 054622 (2012).
[10] A. A. Cowley, G. J. Arendse, J. W. Koen, W. A. Richter, J. A. Stander, G. F. Steyn, P. Demetriou, P. E. Hodgson, and Y. Watanabe, Phys. Rev. C **54**, 778 (1996).
[11] J. V. Pilcher, A. A. Cowley, D. M. Whittal, and J. J. Lawrie, Phys. Rev. C **40**, 1937 (1989).
[12] H. O. Meyer, P. Schwandt, W. W. Jacobs, and J. R. Hall, Phys. Rev. C **27**, 459 (1983).
[13] D. M. Whittal, A. A. Cowley, J. V. Pilcher, S. V. Förtsch, F. D. Smit, and J. J. Lawrie, Phys. Rev. C **42**, 309 (1990).
[14] H. Feshbach, A. Kerman, and S. Koonin, Ann. Phys. (NY) **125**, 429 (1980).
[15] P. D. Kunz and E. Rost, in *Computational Nuclear Physics*, edited by K. Langanke *et al*. (Springer-Verlag, Berlin, 1993), Vol. 2, Chap. 5.
[16] W. A. Richter, A. A. Cowley, G. C. Hillhouse, J. A. Stander, J. W. Koen, S. W. Steyn, R. Lindsay, R. E. Julies, J. J. Lawrie, J. V. Pilcher, and P. E. Hodgson, Phys. Rev. C **49**, 1001 (1994).
[17] P. Huber and K. P. Meyer, in *Proceedings of the International Symposium on Polarization Phenomena of Nucleons, Basel, 4–8 July, 1960*, edited by P. Huber and K. P. Meyer (Birkhauser Verlag, Basel, 1961).
[18] H. H. Barschall and W. Haeberli, in *Proceedings of the Third International Symposium on Polarization Phenomena in Nuclear Reactions, Madison, Wisconsin, USA, 1970* (University of Wisconsin Press, Madison, 1971).
[19] R. Bonetti, L. Colli Milazzo, I. Doda, and P. E. Hodgson, Phys. Rev. C **26**, 2417 (1982).
[20] V. K. Lukyanov, E. V. Zemlyanaya, and K. V. Lukyanov, *JINR Preprint P4-2004-115, Dubna* (Joint Institute for Nuclear Research, Dubna, 2004); Phys. At. Nucl. **69**, 240 (2006).
[21] J. W. Negele and D. Vautherin, Phys. Rev. C **5**, 1472 (1972).
[22] D. T. Khoa and G. R. Satchler, Nucl. Phys. A **668**, 3 (2000).
[23] J. D. Patterson and R. J. Peterson, Nucl. Phys. A **717**, 235 (2003).
[24] M. El-Azab and G. R. Satchler, Nucl. Phys. A **438**, 525 (1985).
[25] V. V. Burov and V. K. Lukyanov, *JINR Preprint P4-11098* (Joint Institute for Nuclear Research, Dubna, 1977).
[26] R. J. Glauber, *Lectures in Theoretical Physics* (Interscience, New York, 1959), p. 315.
[27] S. K. Charagi and S. K. Gupta, Phys. Rev. C **41**, 1610 (1990); **46**, 1982 (1992).
[28] P. Shukla, arXiv:nucl-th/0112039.
[29] G. D. Alkhazov, S. L. Belostotsky, and A. A. Vorobyov, Phys. Rep. **42**, 89 (1978).
[30] K. V. Lukyanov, *Comm. JINR, P11-2007-38, Dubna* (Joint Institute for Nuclear Research, Dubna, 2007).
[31] P. Shukla, Phys. Rev. C **67**, 054607 (2003).
[32] K. V. Lukyanov, V. K. Lukyanov, E. V. Zemlyanaya, A. N. Antonov, and M. K. Gaidarov, Eur. Phys. J. A **33**, 389 (2007).
[33] V. K. Lukyanov, E. V. Zemlyanaya, K. V. Lukyanov, D. N. Kadrev, A. N. Antonov, M. K. Gaidarov, and S. E. Massen, Phys. Rev. C **80**, 024609 (2009).
[34] V. K. Lukyanov, D. N. Kadrev, E. V. Zemlyanaya, A. N. Antonov, K. V. Lukyanov, and M. K. Gaidarov, Phys. Rev. C **82**, 024604 (2010).
[35] V. K. Lukyanov, D. N. Kadrev, E. V. Zemlyanaya, A. N. Antonov, K. V. Lukyanov, M. K. Gaidarov, and K. Spasova, Phys. Rev. C **88**, 034612 (2013).
[36] J. C. Sens and R. J. De Meijer, Nucl. Phys. A **407**, 45 (1983).
[37] E. Gadioli, E. Gadioli–Erba, P. Guazzoni, P. E. Hodgson, and L. Zetta, Z. Phys. A **318**, 147 (1984).
[38] R. Bonetti, F. Crespi, and K.-I. Kubo, Nucl. Phys. A **499**, 381 (1989).
[39] W. R. Falk, R. Abbeg, and S. K. Datta, Nucl. Phys. A **334**, 445 (1980).